Crustal structure across the Kunlun fault from passive source seismic profiling in East Tibet

Tao Xu [a,*], Zhenbo Wu [a,b], Zhongjie Zhang [a], Xiaobo Tian [a], Yangfan Deng [a,b,c], Chenglong Wu [a,b], Jiwen Teng [a]

[a] State Key Laboratory of Lithosphere Evolution, Institute of Geology and Geophysics, Chinese Academy of Sciences, Beijing, 100029, China
[b] University of Chinese Academy of Sciences, Beijing 100049, China
[c] Guangzhou Institute of Geochemistry, Chinese Academy of Sciences, Guangzhou, 510640, China

ABSTRACT

The crust beneath the northeastern (NE) Tibetan Plateau records the imprints on Paleozoic Kunlun orogen and far field effects from continental collision and convergence between the Indian and Eurasian plates. A passive source seismic profile was conducted across eastern Kunlun mountains (also called Animaqing suture belt). Receiver function imaging and H-k stacking results with this dataset demonstrate that (1) crust slightly thins from about 64 km under the Songpan–Ganzi terrane to about 56–62 km under the Qaidam–Kunlun block and the Qilian block; (2) Moho topography is relatively smooth with gradual undulation beneath east Kunlun orogeny belt, in contrast to 2–5 km Moho step at the AKMS/Kunlun fault from previous deep seismic soundings or even no Moho topography variation from recent deep seismic reflection profiling; (3) the average crustal Vp/Vs ratios display an increasing trend to the Kunlun fault belt from 1.76 to 1.85 in Songpan–Ganzi terrane, while decreases from 1.83 to 1.65 away from the fault belt in Qaidam–Kunlun block; (4) The high Vp/Vs ratio in Songpan–Ganzi terrane, is similar to previous results from the profile across Longmenshan fault belt. The normal to low Vp/Vs ratio distribution in Qaidam–Kunlun block supports the viewpoint that the deformation occurring in NE Tibet is predominated by upper-crustal thickening; and (5) the thickness of non-seismogenic layer varies slightly about 40 km between 90° and 100°E, then decreases to less than 20 km around 106°E along the Kunlun fault. The change of the non-seismogenic layer thickness is consistent with the change of the lower crust thickness derived from deep seismic sounding. The increased crustal thickness may be due to the differences in the thickness of the crust of the two plates before their collision, and/or largely achieved by thickening of the lower crust, perhaps indicating a crust flow mechanism operating more strongly in the western region.

© 2013 Elsevier B.V. All rights reserved.

1. Introduction

The formation of the Tibetan plateau is generally attributed to a series of complex accretionary collision events (Molnar et al., 1993; Tapponnier et al., 2001; Yin and Harrison, 2000). Several geodynamic models have been proposed to describe the uplift and outgrowth of the plateau. Kunlun fault is an important boundary featured by flat topography with an altitude of ~5000 m to the south and basins separating by ranges with an average altitude of ~3000 m to the north. A coherent viewpoint, however, has not been obtained on how the two blocks have been juxtaposed at the Kunlun fault. Both northward and southward subductions beneath Kunlun fault have been suggested by various studies (Arnaud et al., 1992; Deng, 1997; Kind et al., 2002; Pearce and Mei, 1988; Tapponnier et al., 2001; Xu et al., 1992; Yin and Harrison, 2000; Zhang et al., 2010a,b,c).

Better knowledge of the crustal structure of the eastern Kunlun mountains along the northeastern boundary of the Tibetan plateau could have a significant impact on understanding the Indian–Asian

collision and the Tibetan plateau formation. Although a number of active and passive source seismic surveys have been carried out in the northeastern Tibetan plateau over the last decade (Galvé et al., 2002; Jiang et al., 2006; Liu et al., 2006; Vergne et al., 2002; Wang et al., 2013; Yuan and hua, 1996; Zhang et al., 2010a, 2011; Zhao et al., 2008), the large shot-receiver intervals that have been used in most of these active seismic acquisition programs can only provide a first-order estimation of the characteristics of the crustal structure. In eastern Tibet, high complicated patterns of fault systems have developed over the course of multiple orogenic events. Hence, more detailed studies of crustal structure in east Tibet is profitable for our understanding of crustal deformation and plateau growth mechanisms. This was the motivation to carry out a passive source seismic survey line which starts from the Songpan–Ganzi terrane, crosses the Qaidam–Kunlun block, and goes eastward into the Qilian block (Fig. 1).

2. Tectonic setting

The Songpan–Ganzi terrane and the Qaidam–Kunlun blocks are separated by the Animaqing–Kunlun–Muztagh suture (AKMS). The Songpan–Ganzi block is a triangular tectonic unit that lies between

---

* Corresponding author.
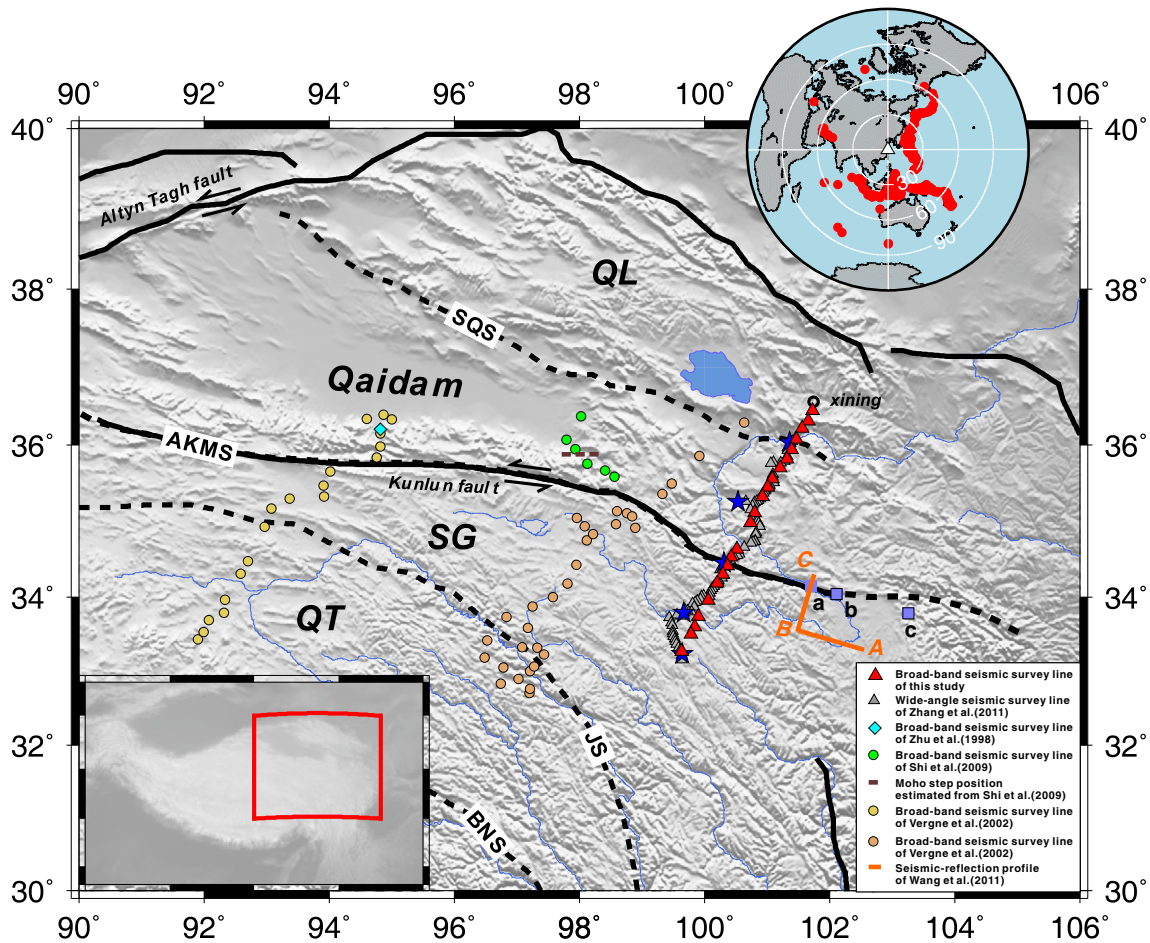   *E-mail address:* xutao@mail.iggcas.ac.cn (T. Xu).

Fig. 1. Tectonic and location map of the seismic stations across the eastern Kunlun Mountains. The red triangles denote the seismic broad-band stations used in this study. The blue stars and gray triangles denote active source seismic shots and receivers for the survey of (Zhang et al., 2011). The top pattern shows the distribution of selected teleseismic events used in this study. The sutures are denoted by BNS: Bangong–Nujiang suture, JS: Jinsha suture, AKMS: Animaqing–Kunlun–Muztagh suture, SQS: South Qilian suture, NQS: North Qilian suture; The terranes or blocks are denoted by SG: Songpan–Ganzi, Qaidam: Qaidam–Kunlun, QL: Qilian. The upper inset shows the distribution of selected teleseismic events used in this study. The lower inset shows the location of Fig. 1 relative to the topography of the Tibet region.

the Qaidam–Kunlun block in the north, the Qiangtang Block in the south and Sichuan basin in the east (e.g. Zhang et al., 2010a,b,c). Qilian block lies in the north of Qaidam–Kunlun block, separated by South Qilian suture (SQS). The location of the passive source seismic survey line and earlier seismic profiles is shown in Fig. 1.

The Kunlun fault, which follows the trace of the AKMS, represents one of the key structural elements in the active deformation field of Eurasia (Avouac and Tapponnier, 1993). The Kunlun Fault has produced five $M > 7.0$ earthquakes in the past century, most recently the M8.1 Kokoxili quake on 11/14/2001 produced a 430 km surface rupture (Fu et al., 2005). The fault marks the northern boundary of the Tibetan Plateau for nearly 1500 km along strike, delineating a transition from a continuous, low-relief, high-elevation plateau to the south to a northern domain characterized by active high mountain ranges and intramontane basins (Kirby et al., 2007). The AKMS represents a complex history of suturing of the Qaidam–Kunlun block to each other in the Late Proterozoic and Paleozoic, and collectively to the Songpan–Gangzi block during the Triassic (Yang et al., 1996). The East Kunlun fault system only became active as a strike–slip system during the last 7 Ma, with a total slip of 75 km (Fu and Awata, 2007) and a late Quaternary slip rate of >10 mm/yr in the west to <2 mm/yr at the tip in the east (Kirby et al., 2007; van der Woerd

et al., 2000, 2002). The Animaqing suture is considered to be a Paleo-tethys oceanic subduction zone that dipped northward in the late Paleozoic (Elena et al., 2003). Other geological mapping and geochemical studies have suggested that the east Kunlun southern marginal ophiolite belt represents a Permian–Triassic ocean (Jiang et al., 2000; Wang et al., 1997; Xu et al., 1992; Yang et al., 1996; Zhu and Helmberger, 1998), or a Carboniferous Paleotethyan Ocean (Bian et al., 2004).

Some details of the character of Moho topography and crustal structure have been derived by previous studies in the surrounding area of the Kunlun fault. Zhu and Helmberger (1998) revealed a 15- to 20-km Moho offset at the southern margin of Qaidam basin by observing anomalous double-pulse teleseismic P-wave arrivals at one station (cyan diamond in Fig. 1). A sharp offset of ~15 km in the Moho depth is observed in a profile using common conversion point (CCP) stacking migration of the P-wave receiver functions at the easternmost of Qaidam basin and Kunlun boundary (Shi et al., 2009, green circles in Fig. 1). Whereas, no Moho topography variation is observed across the eastern and end part of the Kunlun fault from recent deep seismic reflection profiling (Wang et al., 2011). The P-wave velocity gradient in the Songpan–Ganzi terrane agrees well with that of the global average for continental crust from deep seismic profiling (Zhang et al.,
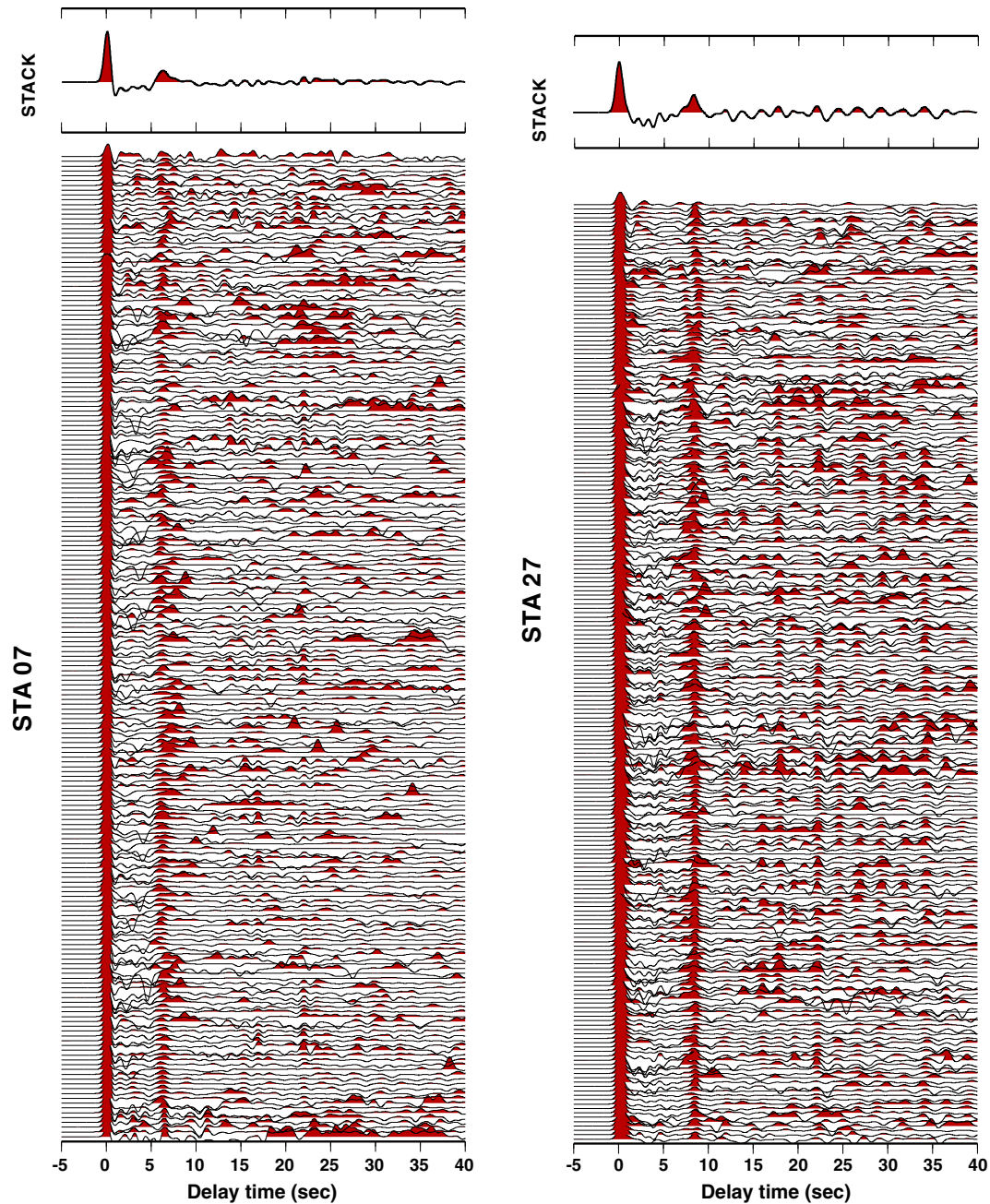
Fig. 2. Radial receiver functions of station 07 (a) and station 27 (b) which are located at Qaidam–Kunlun and Songpan–Ganzi terrane, respectively. The traces are move-out corrected, equally spaced and, for each station, ordered by increasing back-azimuth. The Moho is seen on almost all the traces and the summed trace at the top of the corresponding figure.

2011). Our passive source seismic profile crosses the AKMS zone and the Kunlun fault (Fig. 1) and provides a new opportunity to examine the crustal structure of these tectonic units.

3. Passive source seismic profile and crustal structure from receiver functions

3.1. Seismic acquisition and receiver function image

Our passive seismic experiment was carried out from Songpan–Ganzi terrane to Qilian block (Fig. 1) between November 2010 and June 2011. In this experiment, 22 seismographs (Reftek-72A data loggers and Guralp CMG3-ESP sensors with 50 Hz–30 s bandwidth, Red triangles in Fig. 1) were deployed with interval of about 10–15 km. Stations S00–S04 are located in the Qianlian block, S05–S16 in

the Qaidam–Kunlun block, and S17–S27 in the Songpan–Ganzi terrane. During the six months observation, 805 earthquakes (earthquake catalogue from USGS) with magnitude greater than Ms 5.0 in the epicentral distance range between 30 and 90 degrees (top inset in Fig. 1) were recorded.

The teleseismic direct-P waveform is followed by S waves generated by P-to-S conversion at velocity discontinuities in the crust and upper mantle beneath the seismic stations. Receiver functions are the radial waveforms created by deconvolving the vertical component from the radial component to isolate the receiver site effects from other information contained in the teleseismic P waveforms (Ammon, 1991).

To calculate the receiver functions, we select teleseismic P waveforms from earthquakes with magnitudes Mw ≥ 5.0 and in the epicentral distance range of 30–90°. After rotating the three observed Z, N, and E components to Z, R (radial direction), and T (transverse direction)
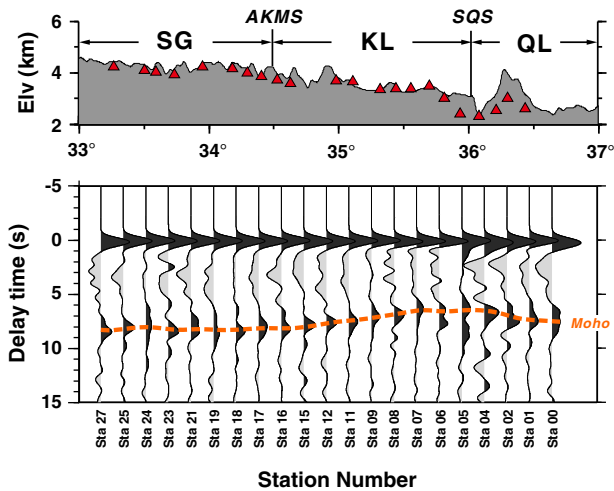
Fig. 3. The summed trace of 22 stations along the profile. The phase indicating Moho (dashed line) is clear and varied along the profile.

components, we calculated receiver functions using a time-domain iterative deconvolution of vertical from radial seismograms (Ligorria and Ammon, 1999; Zhu and Kanamori, 2000). We have visually selected records with high signal-to-noise (S/N) ratio for each station, ensuring that the P-to-S conversions from the Moho and its two later multiple phases are present. Based on a band-pass filter to the raw data with a bandwidth from 0.01 to 1 Hz, we have also applied a low-pass Gauss filter with the coefficient 2.5 to remove high-frequency noise in receiver function. After removing receiver functions with poor signal–noise ratio, we obtained a total of 3436 high-quality receiver functions for all 22 stations along the profile. We present radial-component receiver functions from Stations S07 and S27 located in Qilian block and Songpan–Ganzi terrane, respectively (in Fig. 2a and b). The P and P-to-S phases from the Moho can be seen clearly from those receiver-functions along the profile. The delay time between P and P-to-S converted phases from the Moho under the Qilian block and the Songpan–Ganzi terrane is about 7–8 s. The mild change in delay time from Qilian to Songpan–Ganzi suggests a mild variation in crustal structure along the profile. The stacks of P-receiver functions along the profile clearly indicate that the Moho signature shallows from Songpan–Ganzi to SQS and then deepens to Qilian (Fig. 3).

3.2. Migrated receiver function image along the profile

3.2.1. Migration scheme method

We produce images of the seismic discontinuities in the crust and upper mantle along the profile (Fig. 1) using common conversion point (CCP) stacking of the P wave receiver functions (e.g., Dueker and Sheehan, 1998; Tian et al., 2011; Wu et al., 2005; Yuan et al., 1997). The procedure consists of two steps: back projection and stacking. In the first step, we calculate the ray paths of the receiver functions using a background velocity model. The amplitude at each point on the receiver function is assigned to the corresponding location on the ray path where the P-to-S conversion occurred, using its time delay with respect to the direct P-wave. This amplitude represents the velocity change, or more precisely the impedance change, of the medium at the conversion point. Second, we divide the volume along the profile into certain size bins and sum all amplitudes in each bin to obtain the average amplitude. During this process, the surface topography is taken into account to correct the ray path and the delay time of the conversion phases after the direct P-wave. The delay time produced by the elevation from topography to the sea-level should be removed from the original delay time.

The IASP91 model (Kennett and Engdahl, 1991) is preferred in the migration; the Vp/Vs velocity ratio is assumed to 1.74 in the crust and the bin size is set to 10 km (horizontally along the profile) by 1 km (vertically).

3.2.2. Short description of migrated section of the profile

Fig. 4 presents the migrated receiver-function section to the depth of 120 km along the profile, which demonstrates crustal seismic conversion signatures beneath the Songpan–Ganzi terrane, Qaidam–Kunlun block and the Qilian block. A clear positive phase, interpreted as the Moho P-to-S conversion signal, can be recognized at a depth of 56–64 km along the profile. The Moho P-to-S conversion phase deepens to about 64 km at about 33.2° N.

3.3. Crustal Vp/Vs ratio from H-k stacking along the profile

We have estimated the Moho depth and average crustal Vp/Vs ratio using the H-k stacking method (Zhu and Kanamori, 2000), in which we have summed the amplitudes of receiver functions at predicted arrival times of P-to-S converted phase and its multiples in order to improve signal to noise ratio. A typical velocity of 6.3 km/s was preferred for the average Vp. We use Pms and multiple events (Ppps, Ppss) to stack receiver functions with weighted coefficients of 0.7, 0.2 and 0.1
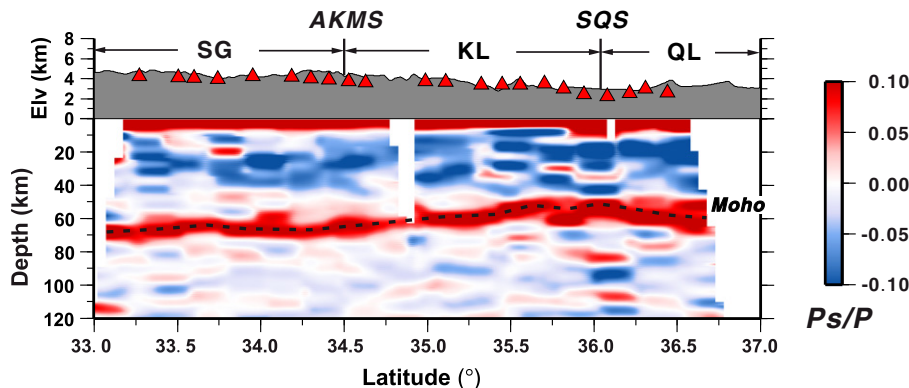

Fig. 4. The topography along the profile and PS migration by the IASP91 model and average crustal Vp/Vs ratio of 1.74. Red colors represent positive receiver-function amplitudes, which are related to the increase of velocity with depth, and blue colors indicate negative amplitudes. The dashed black line denotes estimated Moho depth along the profile.
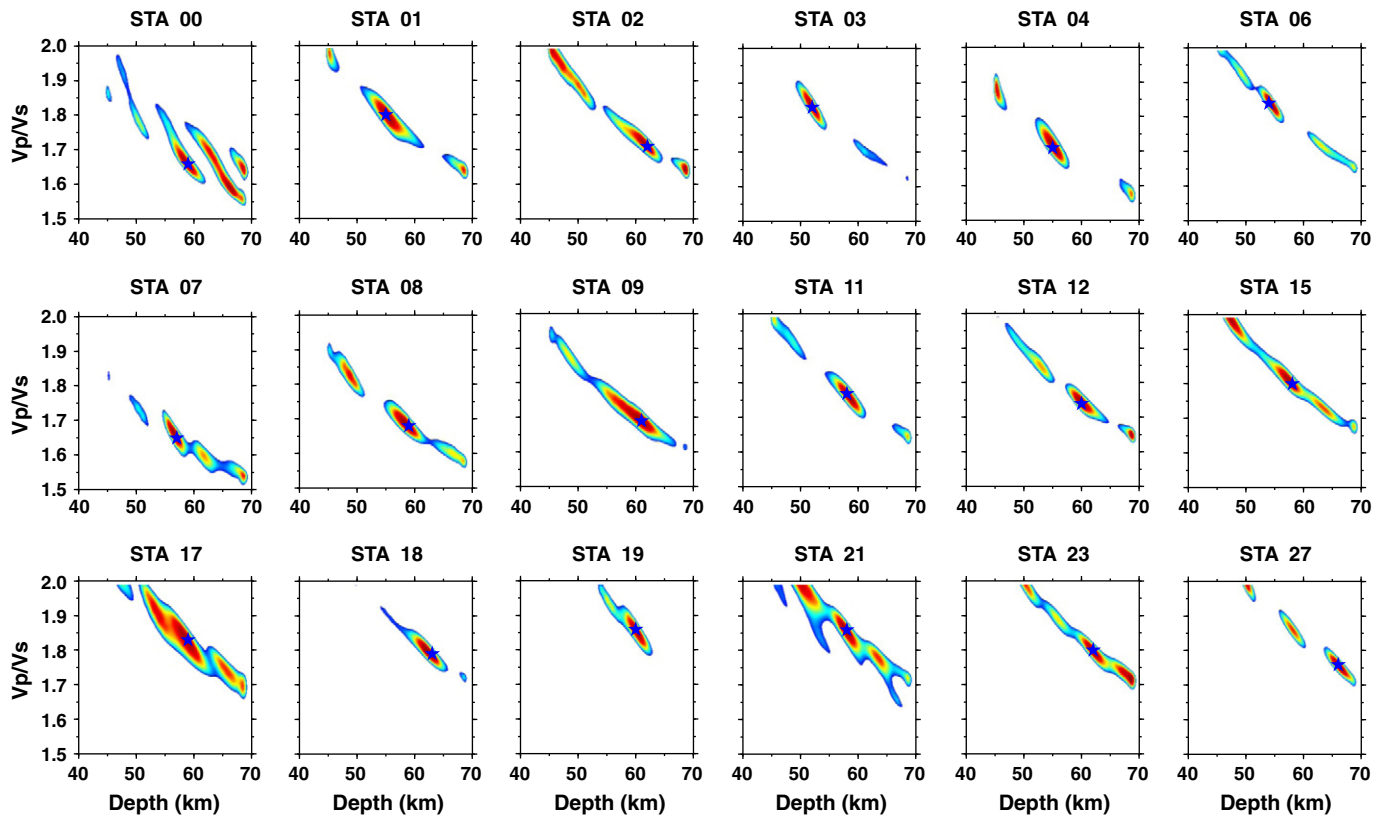
Fig. 5. Average crustal Vp/Vs ratio and Moho depth of 18 stations estimated by the H-k stacking methods. Note that all the figures are in the same color scale.

respectively. The estimated Moho depths of individual stations are also chosen with reference to the CCP migration stack results. The possible Moho depth and crustal Vp/Vs ratio below 18 stations are shown in Fig. 5. Fig. 6 shows the variation of crustal Vp/Vs ratio and its errors (blue error segment) and Moho depth undulation and its errors (red error segment) along the profile. Relatively high values of the Vp/Vs

ratio are observed under the Songpan–Ganzi terrane (1.76–1.85), which are similar to the results in eastern Songpan–Ganzi terrane in the profile across LMS belt (1.75–1.85; Zhang et al., 2009), compared to values in the range 1.65–1.83 under Qaidam–Kunlun block.

4. Discussion

4.1. Comparison with previous studies

There are numerous active and passive source seismic profiles across Kunlun fault belt, such as broadband seismic experiments along Lhasa–Golmud (Profile #1 in Fig. 7) and Yushu–Gonghe (Profile #3 in Fig. 7) profiles in Sino–French joint programs (Vergne et al., 2002). From the migrated receiver function section along Lhasa–Golmud profile, Moho depth is about 65–70 km, Vp/Vs ratio is 1.74–1.84 beneath Songpan–Ganzi, and are about 55–65 km and 1.65–1.77 beneath Qaidam–Kunlun block, respectively. Along Yushu–Gonghe profile, Moho depth is about 70 km, Vp/Vs ratio is 1.72–1.74 beneath Songpan–Ganzi, and are about 50–65 km, Vp/Vs ratio is 1.72 beneath Qaidam–Kunlun block (Vergne et al., 2002). From our results, Moho depth is about 56–64 km, Vp/Vs ratio is 1.76–1.85 beneath Songpan–Ganzi, and Moho depth is about 56–62 km, Vp/Vs ratio is 1.65–1.83 beneath Qaidam–Kunlun block. Moho depth derived from passive source seismic profiling shallows from west to east similar to those derived from deep seismic sounding (Fig. 8a, Zhang et al., 2011).

On the two parallel profiles west of the profile of this study, Moho depth deepens from about 50 km near the northern edge of the plateau to about 80 km at the south of the Jinsha suture in the Qiang Tang block (Profile #1 and Profile #3 in Fig. 7). Crustal thickening occurs in stair-case fashion, often with steps located near the main, reactivated sutures. While on the profile of this study, a relatively smooth and gradual Moho topography undulation is beneath the eastern Kunlun orogeny belt.
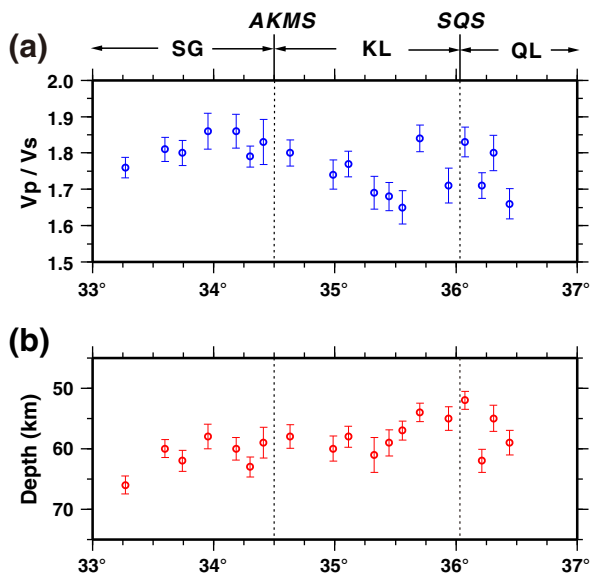

Fig. 6. The value and error of crustal Vp/Vs ratio (blue error segment) and Moho depth (red error segment), plotted for stations along the profile. SG, AKMS, KL, SQS and QL are as in Fig. 1.
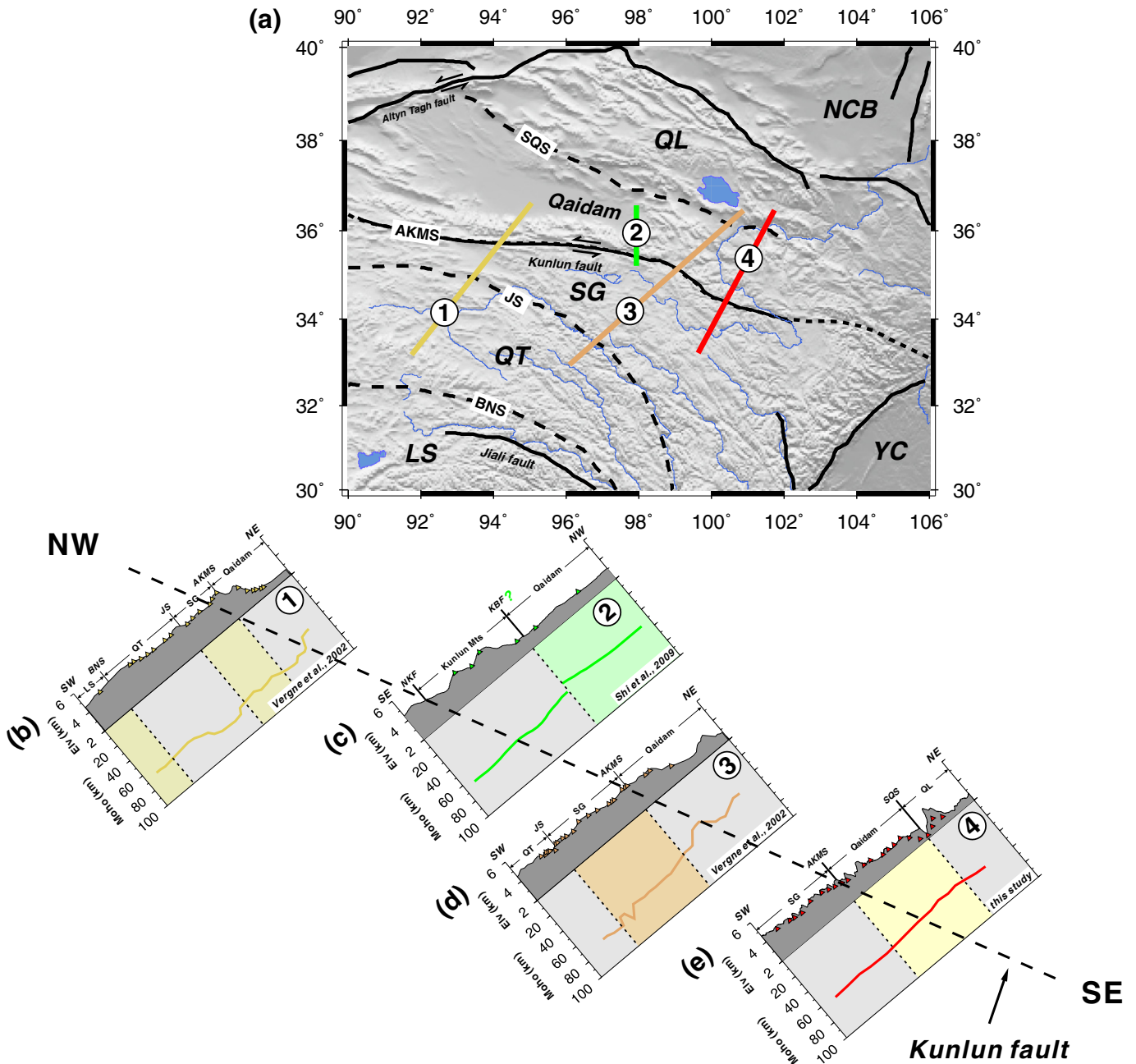
Fig. 7. Comparison of Moho depths derived in this study with those from previous passive-source studies. The Moho depths along the Lhasa–Golmud profile (#1, Fig. b) and along the Yushu–Gonghe profile (#3, Fig. d) by Vergne et al., 2002. The Moho depths across the SG/Qaidam–Kunlun boundary (#2, Fig. c are by Shi et al., 2009). The Moho depth across east Kunlun Mts belt of this study (#4, Fig. e) are from this study.

4.2. Moho beneath Kunlun orogeny belt and distinctive Vp/Vs ratio beneath Songpan–Ganzi and Qaidam–Kunlun blocks

The significant observation of our experiment is the relatively smooth and gradual Moho topography undulation beneath east Kunlun orogeny belt, in contrast to 2–5 km Moho step from previous deep seismic soundings (Fig. 8a) or even no Moho topography variation from recent deep seismic reflection profiling (Fig. 8b). The flat Moho in the nearly vertical reflection profiling in Fig. 8b (Wang et al., 2011) was taken as seismic evidence against lower crustal flow northeast-ward, and the active deforming middle crust was inferred from the distinctive patterns of seismic reflections (Fig. 8b).The Vp/Vs ratio can reveal contrasts in crustal mineralogy and chemical composition, including those related to partial melting, a process which tends to

raise the Vp/Vs ratios (Watanabe, 1993). Laboratory experiments have shown that the Vp/Vs ratio offers better constraints on crustal composition than individual Vp or Vs parameters because the ratio is less sensi-tive to variations in pressure and temperature (Chevrot and van der Hilst, 2000; Christensen, 1996).

The Songpan–Ganzi terrane and the east Qaidam–Kunlun block exhibit distinctly Vp/Vs velocity ratios, indicative perhaps of different crustal compositions, where the Qaidam–Kunlun block has been juxta-posed against Songpan–Ganzi terrane by the AKMS. Considering the rock properties, the higher ratio of Songpan–Ganzi terrane may imply that the crust is less felsic and more mafic. The lower Vp/Vs ratio under Kunlun block, suggests that the crust is more felsic than the subsurface materials of surrounding areas. The result supports that de-formation is occurring in NE Tibet is predominantly by upper-crustal
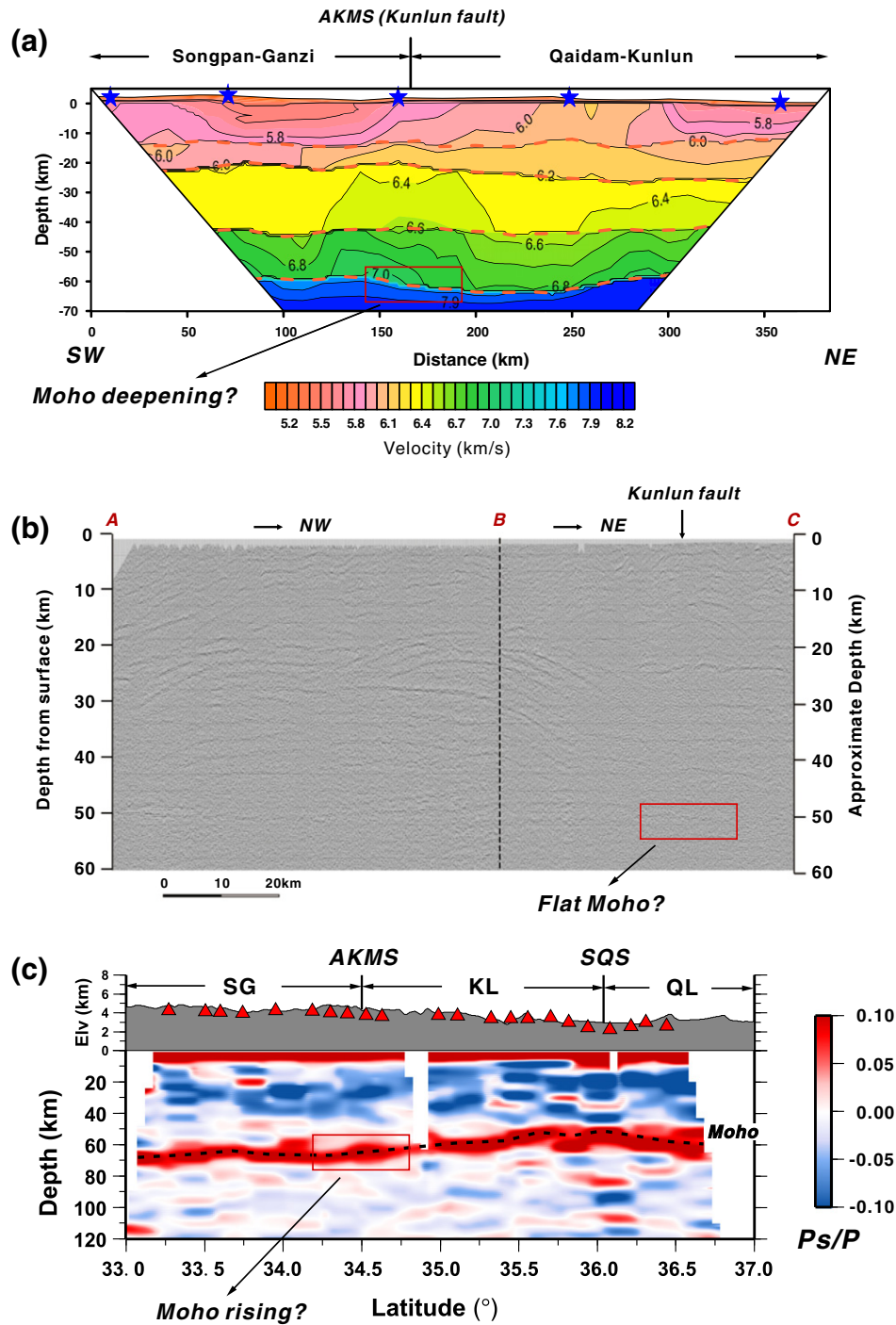
Fig. 8. (a) Crustal velocity model derived from the deep seismic sounding data (Zhang et al., 2011); (b) Moho character from seismic reflection profile (Wang et al., 2011); (c) Moho depth undulation along the profile of this experiment. The cyan lines indicate the seismogenic layer (SL) (within which 80% of the seismic energy is released). The black dashed lines indicate the Moho depth.

thickening, which was inferred from the spatial distribution of crustal thickness and Vp/Vs ratio (Tian and Zhang, 2013).

The composition of the crust has great impact on the Vp/Vs, and also gives some revelation on the rheology (Watts, 2001), as it reflects the flexural rigidity of the rocks. The rheology has been estimated with yield strength envelope and elastic thickness (Deng et al., 2013; Pérez-Gussinyé et al., 2007; Tesauro et al., 2012). While, in the recent years, the rheological properties of the crust could also be quantified using the scheme proposed by Panza and Raykova (2008), i.e., considering

the distribution of the depth of the hypocentres (N) and the seismic energy released E. As a proxy for the rheology, the lack of seismicity does not necessarily imply that the lithosphere is locally more rigid (it may indicate, for example, that there is no active tectonics or that the strain rate is locally lower than in the surroundings) (Panza and Raykova, 2008; Wu and Zhang, 2012; Zhang et al., 2011, 2013). All the seismic events reported during the period 1980 to 2012 in the Catalogue of the China Earthquake Network Center (CENC) below this region were compiled. Consequently, we made 4 contiguous cells along our profile
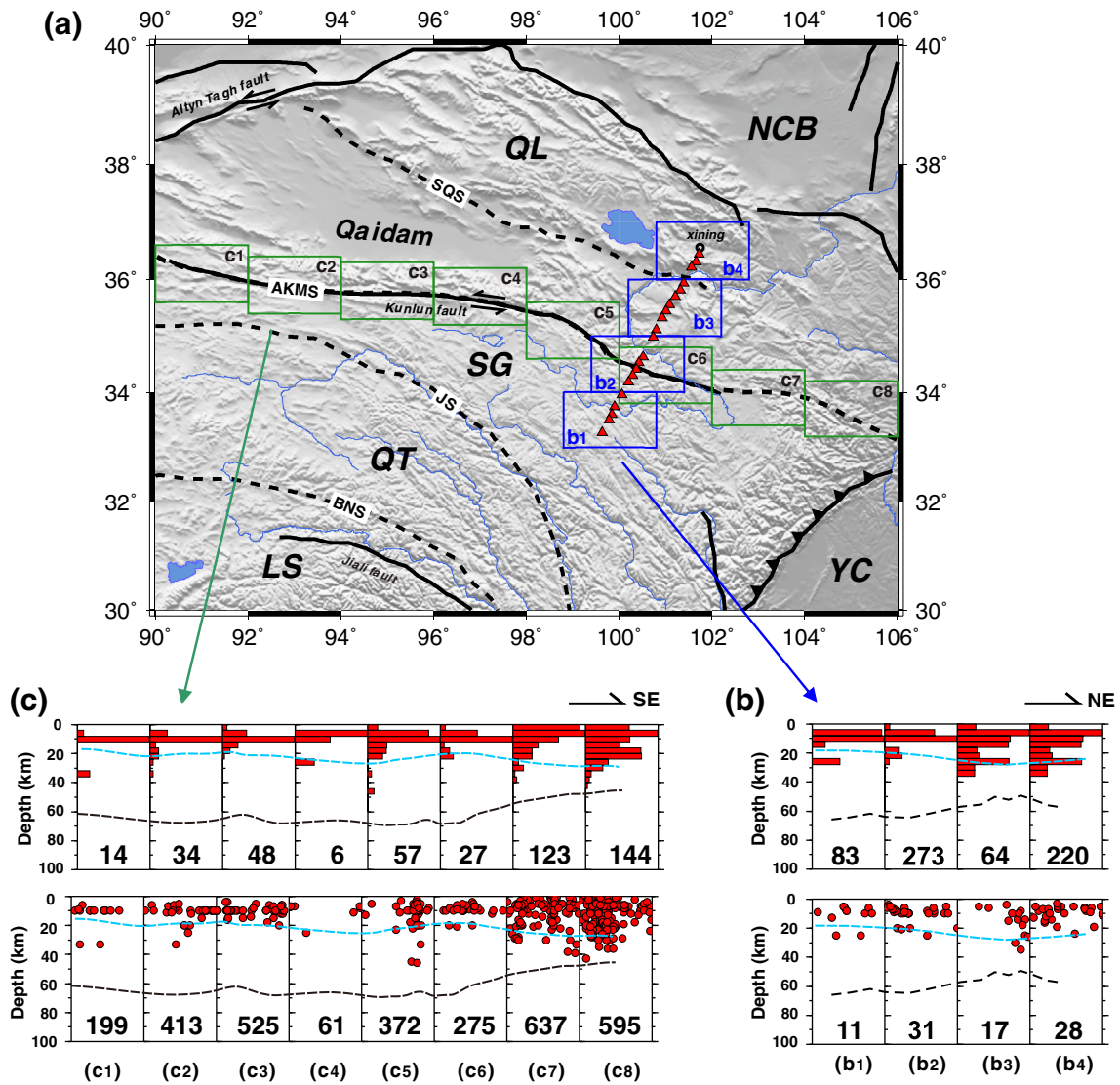
Fig. 9. The earthquake distribution versus depth (upper panel) and the earthquake energy versus depth by 4 km interval (low panel) for 4 cells along our profile (b) and for 8 cells along the Kunlun fault (c). The hypocenters with depth are denoted by red dots. The number at the bottom indicates the hypocenters within each cell. The filled red bars histogram represents the energy of all earthquakes from the catalogue for 1980–2012 provided by China Earthquake Network Center, the maximum value of the energy Emax (used for normalization) is also indicated at the bottom of each cell.

with the sizes of about 2° in longitude and 1° in latitude dimensions (Fig. 9b) to define the distributions of (a) hypocentral depth (h), (b) log E/Emax versus h. Where, seismic energy (E) is inverted from earthquake magnitude (Ms): log$E = 11.8 + 1.5$ Ms (Panza and Raykova, 2008; Zhang et al., 2011; Zhang et al., 2013). The depth at which 80% of earthquake energy is released is termed as seismogenic layer SL (Deng et al., 2012; Panza et al., 2003; Wu and Zhang, 2012; Zhang et al., 2011, 2012, 2013), which reflects the extent of faulting and strength in the uppermost part of the lithosphere. From the 4 cells, we can observe that the earthquakes are concentrated in the upper crust (<30 km) (Gao et al., 2000). And the thickness of SL in b3 and b4 is 10 km thicker than b1 and b2 (about 20 km beneath Songpan–Ganzi and about 30 km beneath Kunlun and Qilian block). As the cell b2 passed through the AKMS, the seismicity here is remarkable stronger than the other three cells. Compared with b1, b3, and b4, we find that region with stronger seismicity corresponds to a low Vp/Vs (Fig. 6), as the cell b4, which is consistent with the thicker seismogenic layer in Qilian block.

4.3. West–east variation of crustal structure and its possible relations with surface deformation

Qaidam–Kunlun block is juxtaposed against the Songpan–Ganzi terrane by the AKMS suture and the Kunlun fault. The Kunlun fault only became active as a strike–slip system during the last 7 Ma, with a total slip of 75 km (Fu and Awata, 2007) and a late Quaternary slip rate of 12 ± 3 mm/yr (van der Woerd et al., 2000). Slip rates decrease systematically along the eastern ~150 km of the fault from >10 to <2 mm/yr (purple rectangles marked with a, b and c in Fig. 1, Kirby et al., 2007; Van der Woerd et al., 2000, 2002).

We made statistics of seismic events in 8 cells with the sizes of about 2° in Longitude and 1° in latitude dimensions along the Kunlun fault in the same way as above (Fig. 9c). The pattern difference of seismic energy release between cells c1 and c8 exhibits significant variation of seismic energy release along the Kunlun fault. From Fig. 9c, we can observe that seismogenic layer varies slightly from less than 20 km in the west (about 90°E) to about 30 km in the east (106°E) along the Kunlun

fault. The Moho depth varies from 60 to 70 km from in the west to less than 50 km in the east (Teng et al., 2013; Zhang et al., 2011). The non-seismogenic layer, the area which is restricted by the lower border of seismogenic zone and Moho, keeps mild change of 40 km from 90° to 100°E, while changes to less than 20 km east of 100°E. The tendency of non-seismogenic layer is consistent with the lower crustal thickness derived from deep seismic sounding (Zhang et al., 2011). The increased crustal thickness may be due to the differences in the thickness of the crust of the two plates before their collision, and/or largely achieved by thickening of the lower crust, perhaps indicating a crustal flow mechanism operating more strongly in the western region.

5. Conclusion

Based on the receiver function imaging and H-k stacking results along the profile in the northern Tibet. Our interpretation of the passive source seismic profiling suggests the following conclusions:

(1) Crustal thickness exhibits a mild variation from ~56 to 62 km under the Qilian block and Qaidam–Kunlun block, to ~64 km under the Songpan–Ganzi terrane.

(2) The distinctive velocity ratio differences across AKMS mark that Kunlun block is juxtaposed against Songpan–Ganzi terrane by the AKMS. The lower Vp/Vs ratio under Qaidam–Kunlun block supports why the deformation occurring in NE Tibet is predominated by upper-crustal thickening (Tian and Zhang, 2013).

(3) The non-seismogenic layer varies slightly from 40 km in 90° to 100°E, then decreases to less than 20 km in 106°E along the Kunlun fault. The tendency of non-seismogenic layer, consistent with the lower crust thickness derived from deep seismic sounding. The increased crustal thickness may be due to the differences in the thickness of the crust of the two plates before their collision, and/or largely achieved by thickening of the lower crust, perhaps indicating a crust flow mechanism operating more strongly in the western region.

References

Ammon, C.J., 1991. The isolation of receiver effects from teleseismic P waveforms. Bull. Seismol. Soc. Am. 81, 2504–2510.
Arnaud, N.O., Vidal, P., Tapponnier, P., Matte, P., Deng, W.M., 1992. The high K2O volcanism of northwestern Tibet: geochemistry and tectonic implications. Earth Planet. Sci. Lett. 111, 351–367.
Avouac, J., Tapponnier, P., 1993. Kinematic model of active deformation in central Asia. Geophys. Res. Lett. 20. http://dx.doi.org/10.1029/93GL00128.
Bian, Q.T., Li, D.H., Pospelov, I., Yin, L.M., Li, H.S., Zhao, D.S., Chang, C.F., Luo, X.Q., Gao, S.L., Astrakhantsev, O., Chamov, N., 2004. Age, geochemistry and tectonic setting of Buqingshan ophiolites, North Qinghai–Tibet Plateau, China. J. Asian Earth Sci. 23 (4), 577–596.
Chevrot, S., van der Hilst, R.D., 2000. The Poisson ratio of the Australian crust: geological and geophysical implications. Earth Planet. Sci. Lett. 183, 121–132.
Christensen, N.I., 1996. Poisson's ratio and crustal seismology. J. Geophys. Res. 101, 3139–3156.
Deng, W.M., 1997. Cenozoic volcanism and lithosphere tectonic evolution in the northern Tibetan plateau, China. In: Li, Z.N., Qi, J.Z., Zhang, Z.C. (Eds.), Igneous Petrology. 30th International Geological Congress, vol. 15, pp. 3–12 (Utrecht, The Netherlands Tokyo, Japan).
Deng, Y., Fan, W., Zhang, Z., Badal, J., 2012. Geophysical evidence on segmentation of the Tancheng-Lujiang fault and its implications on the lithosphere evolution in East China. J. Asian Earth Sci. http://dx.doi.org/10.1016/j.jseaes.2012.11.006.
Deng, Y., Zhang, Z., Fan, W., Pérez-Gussinyé, M., 2013. Multitaper spectral method to estimate the elastic thickness of South China: implications for intracontinental deformation. Geosci. Front. http://dx.doi.org/10.1016/j.gsf.2013.05.002.
Dueker, K.G., Sheehan, A.F., 1998. Mantle discontinuity structure beneath the Colorado Rocky Mountains and High Plains. J. Geophys. Res. 103, 7153–7169.
Elena, A.K., Brunel, M., Malavielle, J., 2003. Discovery of the Paleo-Tethys residual peridotites along the Anyemaqen–KunLun suture zone (North Tibet). Compt. Rendus Geosci. 335 (8), 709.
Fu, B.H., Awata, Y., 2007. Displacement and timing of left-lateral faulting in the Kunlun Fault Zone, northern Tibet, inferred geologic and geomorphic features. J. Asian Earth Sci. 29, 253–265.
Fu, B., Awata, Y., Du, J., Ninomiya, Y., He, W., 2005. Complex geometry and segmentation of the surface rupture associated with the 14 November 2001 great Kunlun earthquake, northern Tibet, China. Tectonophysics 407, 43–63. http://dx.doi.org/10.1016/j.tecto.2005.07.002.
Galvé, A., Hirn, A., Jiang, M., Gallart, J., de Voogd, B., Lepine, J.C., Diaz, J., Wang, Y.X., Qian, H., 2002. Modes of raising northeastern Tibet probed by explosion seismology. Earth Planet. Sci. Lett. 203, 35–43.
Gao, Y., Wu, Z.-L., Liu, Z., Zhou, H.-L., 2000. Seismic source characteristics of nine strong earthquakes from 1988 to 1990 and earthquake activity since 1970 in the Sichuan–Qinghai–Xizang (Tibet) zone of China. Pure Appl. Geophys. 157 (9), 1423–1443.
Jiang, C.F., Wang, Z.Q., Li, J.Y., 2000. Opening-Closing tectonics of the Central Orogenic Belt in China. Geological Publishing House, Beijing (154 pp., in Chinese, with English abstract).
Jiang, M., Galvé, A., Hirn, A., de Voogd, B., Laigle, M., Su, H.P., Diaz, J., Lépine, J.C., Wang, Y.X., 2006. Crustal thickening and variations in architecture form the Qaidam basin to the Qang Tang (North-Central Tibetan Plateau) from wide-angle reflection seismology. Tectonophysics 412, 121–140.
Kennett, B.L.N., Engdahl, E.R., 1991. Traveltimes for global earthquake location and phase identification. Geophys. J. Int. 105 (2), 429–465.
Kind, R., Yuan, X., Saul, J., Nelson, D., Sobolev, S.V., Mechie, J., Zhao, W., Kosarev, G., Ni, J., Achauer, U., Jiang, M., 2002. Seismic images of crust and upper mantle beneath Tibet: evidence for Eurasian Plate subduction. Science 298, 1219–1221.
Kirby, E., Harkins, N., Wang, E., Shi, X., Fan, C., Burbank, D., 2007. Slip rate gradients along the eastern Kunlun fault. Tectonics 26, TC2010. http://dx.doi.org/10.1029/2006TC002033.
Ligorria, J.P., Ammon, C.J., 1999. Iterative deconvolution and receiver function estimation. Bull. Seismol. Soc. Am. 89, 1395–1400.
Liu, M.J., Mooney, W.D., Li, S.L., Okaya, N., Detweiler, S., 2006. Crustal structure of the northeastern margin of the Tibetan plateau from the Songpan-Ganzi terrane to the Ordos basin. Tectonophysics 420, 253–266.
Molnar, P., England, P., Martinod, J., 1993. Mantle dynamics, uplift of the Tibetan plateau and the Indian Monsoon. Rev. Geophys. 31, 357–396.
Panza, G.F., Pontevivo, A., Chimera, G., Raykova, R., Aoudia, A., 2003. The lithosphere-asthenosphere: Italy and surroundings. Episodes-Newsmagazine of the International Union of Geological Sciences 26 (3), 169–174.
Panza, G.F., Raykova, R.B., 2008. Structure and rheology of lithosphere in Italy and surrounding. Terra Nova 20 (3), 194–199.
Pearce, J.A., Mei, H.J., 1988. Volcanic rocks of the 1985 Tibet geotraverse Lhasa to Golmud. The geological evolution of Tibet. Philos. Trans. R. Soc. Lond. 169–201.
Pérez-Gussinyé, M., Lowry, A., Watts, A., 2007. Effective elastic thickness of South America and its implications for intracontinental deformation. Geochem. Geophys. Geosyst. 8 (5), 22.
Shi, D., Shen, Y., Zhao, W., Li, A., 2009. Seismic evidence for a Moho offset and south-directed thrust at the easternmost Qaidam–Kunlun boundary in the Northeast Tibetan plateau. Earth Planet. Sci. Lett. 288, 329–334.
Tapponnier, P., Xu, Z., Roger, F., Meyer, B., Arnaud, N., Wittlinger, G., Yang, J., 2001. Oblique stepwise rise and growth of the Tibet plateau. Science 294, 1671–1677.
Teng, J.W., Zhang, Z.J., Zhang, X.K., Wang, C.Y., Gao, R., Yang, B.J., Qiao, Y.H., Deng, Y.F., 2013. Investigation of the Moho discontinuity beneath the Chinese mainland using deep seismic sounding profiles. Tectonophysics 609, 202–216.
Tesauro, M., Kaban, M.K., Cloetingh, S.A., 2012. Global strength and elastic thickness of the lithosphere. Glob. Planet. Chang. 90, 51–57.
Tian, X., Zhang, Z., 2013. Bulk crustal properties in NE Tibet and their implications for deformation model. Gondwana Res. 24, 548–559. http://dx.doi.org/10.1016/j.gr.2012.12.024.
Tian, X.B., Teng, J.W., Zhang, H.S., Zhang, Z.J., Zhang, Y.Q., Yang, H., 2011. Structure of crust and upper mantle beneath the Ordos Block and the Yinshan Mountains revealed by receiver function analysis. Phys. Earth Planet. Inter. 184, 186–193. http://dx.doi.org/10.1016/j.pepi.2010.11.007.
Van der Woerd, J., Ryerson, F.J., Tapponnier, P., Meriaux, A.S., Gaudemer, Y., Meyer, B., Finkel, R.C., Caffee, M.W., Zhao, G.G., Xu, Z.Q., 2000. Uniform slip-rate along the Kunlun Fault: implications for seismic behaviour and large-scale tectonics. Geophys. Res. Lett. 27, 2353–2356.
Van der Woerd, J., Tapponnier, P., Ryerson, F.J., Meriaux, A.S., Meyer, B., Gaudemer, Y., Finkel, R.C., Caffee, M.W., Zhao, G., Xu, Z., 2002. Uniform postglacial slip-rate along the central 600 km of the Kunlun Fault (Tibet), from ^{26}Al, ^{10}Be, and ^{14}C dating of

riser offsets, and climatic origin of the regional morphology. Geophys. J. Int. 148, 356–388.

Vergne, J., Wittlinger, G., Qiang, H., Tapponnier, P., Poupinet, G., Jiang, M., Herquel, G., Paul, A., 2002. Seismic evidence for stepwise thickening of the crust across the NE Tibetan plateau. Earth Planet. Sci. Lett. 203, 25–33.

Wang, Y.B., Huang, J.C., Luo, M.S., Tian, J., Bai, Y.S., 1997. Paleo-ocean evolution of the southern eastern Kunlun orogenic belt during Hercy-Early Indosinian. Earth Sci. China Univ. Geosci. 22, 369–372 (in Chinese, with English abstract).

Wang, C.S., Gao, R., Yin, A., Wang, H.Y., Zhang, Y.X., Guo, T.L., Li, Q.S., Li, Y.L., 2011. A mid-crustal strain-transfer model for continental deformation: a new perspective from high-resolution deep seismic-reflection profiling across NE Tibet. Earth Planet. Sci. Lett. 306, 279–288.

Wang, Y.X., Mooney, W., Yuan, X.C., Okaya, N., 2013. Crustal structure of the Northeastern Tibetan Plateau from the Southern Tarim basin to the Sichuan Basin, China. Tectonophysics 584, 191–208.

Watanabe, T., 1993. Effects of water and melt on seismic velocities and their application to characterization of seismic reflectors. Geophys. Res. Lett. 20, 2933–2936.

Watts, A.B., 2001. Isostasy and Flexure of the Lithosphere. Cambridge University Press.

Wu, J., Zhang, Z.J., 2012. Spatial distribution of seismic layer, crustal thickness, and Vp/Vs ratio in the Permian Emeishan Mantle Plume region. Gondwana Res. 22, 127–139.

Wu, Q.J., Zeng, R.S., Zhao, W.J., 2005. The upper mantle structure of the Tibetan Plateau and its implication for the continent–continent collision. Sci. China Ser. D 48, 1158–1164.

Xu, Z.Q., Hou, L.W., Wang, Z.X., Fu, X.F., Huang, M.H., 1992. Orogenic Processes of the Songpan–Ganze Orogenic Belt of China. Geological Publishing House, Beijing (in Chinese).

Yang, J.S., Robinson, P.T., Jiang, C.F., Xu, Z.Q., 1996. Ophiolites of the Kunlun Mountains, China and their tectonic implications. Tectonophysics 258, 215–231.

Yin, A., Harrison, T.M., 2000. Geologic evolution of the Himalayan–Tibetan orogen. Annu. Rev. Earth Planet. Sci. 28, 211–280.

Yuan, X.C., Hua, J.R., 1996. Geophysics Atlas of China. Geology Press, Beijing 135–144.

Yuan, X., Ni, J., Kind, R., Mechie, J., Sandvol, E., 1997. Lithospheric and upper mantle structure of southern Tibet from a seismological passive source experiment. J. Geophys. Res. 102, 27,491–27,500. http://dx.doi.org/10.1029/97JB02379.

Zhang, Z.J., Wang, Y., Chen, Y., Houseman, G.A., Tian, X., Wang, E., Teng, J., 2009. Crustal structure across Longmenshan fault belt from passive source seismic profiling. Geophys. Res. Lett. 36, L17310. http://dx.doi.org/10.1029/2009GL039580.

Zhang, Z.J., Yuan, X.H., Chen, Y., Tian, X.B., Kind, R., Li, X.Q., Teng, J.W., 2010a. Seismic signature of the collision between the east Tibetan escape flow and the Sichuan Basin. Earth Planet. Sci. Lett. 292, 254–264.

Zhang, Z.J., Deng, Y.F., Teng, J.W., Wang, C.Y., Gao, R., Chen, Y., Fan, W.M., 2010b. An overview of the crustal structure of the Tibetan plateau after 35 years of deep seismic soundings. J. Asian Earth Sci. http://dx.doi.org/10.1016/j.jseaes.2010.03.010.

Zhang, C., Yang, D., Wang, H., Takahashi, Y., Ye, H., 2010c. Neoproterozoic maficultramafic layered intrusion in Quruqtagh of northeastern Tarim Block, NW China: two phases of mafic igneous activity with different mantle resources. Gondwana Res. http://dx.doi.org/10.1016/j.gr.2010.03.012.

Zhang, Z.J., Klemperer, S., Bai, Z.M., Chen, Y., Teng, J.W., 2011. Crustal structure of the Paleozoic Kunlun orogeny from an active-source seismic profile between Moba and Guide in East Tibet, China. Gondwana Res. 19, 994–1007.

Zhang, Z., Wu, J., Deng, Y., Teng, J., Zhang, X., Chen, Y., Panza, G., 2012. Lateral variation of the strength of lithosphere across the eastern North China Craton: New constraints on lithospheric disruption. Gondwana Research 22 (3), 1047–1059.

Zhang, Z., Deng, Y.F., Chen, L., Wu, J., Teng, J.W., Panza, G., 2013. Seismic structure and rheology of the crust under mainland China. Gondwana Res. 23, 1455–1483.

Zhao, W.J., Brown, L., Wu, Z., Klemperer, S.L., Shi, D., Mechie, J., Su, H., Tilmann, F., Karplus, M.S., Makovsky, Y., 2008. Seismology Across the Northeastern Edge of the Tibetan Plateau. EOS Trans. Am. Geophys. Union 89 (48), 487.

Zhu, L.P., Helmberger, L.V., 1998. Moho offset across the northern margin of Tibetan plateau. Science 281, 1170–1172.

Zhu, L.P., Kanamori, H., 2000. Moho depth variation in southern California from teleseismic receiver functions. J. Geophys. Res. 105, 2969–2980. http://dx.doi.org/10.1029/1999JB900322.